Materials Chemistry and Physics 337 (2025) 130597

Contents lists available at ScienceDirect

Materials Chemistry and Physics

journal homepage: www.elsevier.com/locate/matchemphys

Synergistic effects of graphene nanosheets on the microstructure, hardness and tribological performance of Al/WC nanocomposites fabricated by flake powder metallurgy

Mohsen Saremi Ghareh Gol, Abolfazl Malti, Farshad Akhlaghi *

School of Metallurgy and Materials Engineering, Faculty of Engineering, University of Tehran, P.O.Box: 11155-4563, Tehran, Iran

HIGHLIGHTS

- Al-WC-graphene nanocomposite Synthesized via a novel PM method.
- The influence of GNSs content and fabrication route on properties of composites Investigate.
- Optimal porosity and hardness achieved with 6 h of milling.
- Higher GNSs contents improve wear resistance at higher loads.
- Formation of Tribolayer increases with load, distance, and GNS content.

ARTICLE INFO

Keywords:
Nanocomposites
Aluminum
Graphene
Tribology
Tribolayer
Nanostructure

ABSTRACT

This research investigates the characteristics of a newly developed Al-WC-graphene nanocomposite, fabricated via flake powder metallurgy (FPM) technique. For exploring the best root for a successful graphene nanosheets (GNSs) dispersion, two distinct mixing procedure examined. The effects of GNS concentration and FPM processing parameters on the microstructure, porosity, hardness, fracture and dry sliding wear behavior of the produced nanocomposites were studied by XRD, FESEM, OM, density measurement, hardness measurement and pin-on-disk wearing test techniques. Findings revealed that 6 h of concurrent milling produced optimal porosity and hardness. While increasing GNSs content led to decreased density, addition of 0.5 vol% of GNSs improved the microhardness by up to 105 % as compared to that of the reference sample. Analysis of the fracture surfaces indicated diminishing of the composite's ductility by graphene addition. The nanocomposite containing 0.5 vol% of GNSs demonstrated superior wear resistance (up to 38 % improvement) under low loads and distances, whereas 1 vol% GNSs addition enhanced tribological performance (up to 33 % improvement) at higher loads and distances. These results attributed to formation of a protective tribo-layer that provided insights into the underlying wear mechanisms.

1. Introduction

Aluminum matrix composites (AMCs) due to their superior physical and mechanical properties are increasingly utilized in many industrial applications. Among these, hybrid composites, containing two or more reinforcements, have received particular attention [1,2]. Examples of this type of composites include those containing ceramic particles for strength, along with a lubricating phase such as graphite or graphene nano sheets (GNSs) distributed in the matrix alloy [3].

Recently considerable research attempts have been made to synthesize and characterize the physical and mechanical performances of Al matrix composites having the potential for satisfying the modern needs of various industrial and technological applications such as automotive, aerospace, sports, and electronics, due to their excellent properties [4,5].

Graphene due to its suitable physical and mechanical features such as high hardness, great strength and stiffness, desirable abrasion properties as well as good corrosion resistance have witnessed tremendous growth for serving as a reinforcing material for Al alloys [6]. Previous research by Mahdavi et al. explored the fabrication and properties of a

* Corresponding author.
E-mail address: fakhlagh@ut.ac.ir (F. Akhlaghi).

https://doi.org/10.1016/j.matchemphys.2025.130597
Received 23 September 2024; Received in revised form 13 December 2024; Accepted 22 February 2025
Available online 25 February 2025

Table 1
Chemical composition (wt. %) of Al powders used in this study.

Fe	Si	Pb	Cu	Sb	Zn	Mn	Sn	Al
0.34	0.216	0.072	0.044	0.044	0.036	0.031	0.024	Balance

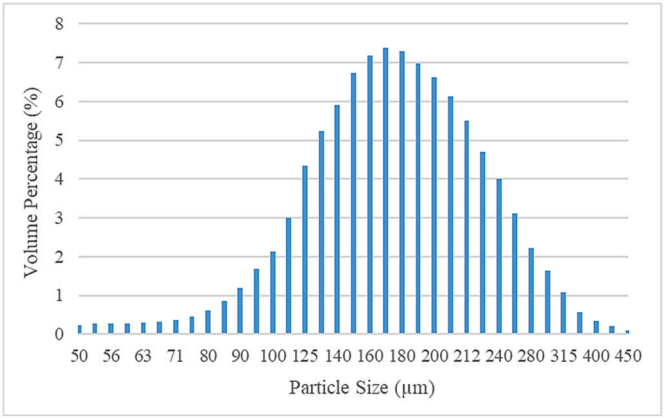

Fig. 1. Al particle size distribution.

hybrid Al–SiC-Graphite composite using a novel in-situ powder metallurgy (IPM) route. Their study revealed a complex effect of the graphite-lubricating phase, exhibiting both positive (surface lubrication) and negative (reduced hardness) impacts. However, this negative effect was compensated by SiC addition that maintained hardness [7]. GNSs with their potential for similar lubrication capability without compromising hardness, present a promising alternative for enhancing the performance of such composites.

As previously reported in several studies [8–10], a significant challenge in metal matrix composites is the increased porosity that is often accompanied by the addition of reinforcements [11]. Mosleh-Shirazi et al. explored the effect of nano- and micro-sized SiC particles on the characteristics of Al–SiC composites. They observed that nano-sized reinforcements resulted in higher hardness and lower porosity as compared to micro-sized reinforced samples. These findings highlight the potential benefits of utilizing nano-sized reinforcements to overcome the porosity challenge in AMCs [12]. In a study by Ahmadian et al., Mg–Ti–SiC composites fabricated via powder metallurgy. A significant decrease in Mg crystallite size was observed in samples containing nano-sized SiC as compared to those reinforced with micro-sized SiC [13]. Tungsten carbide (WC) due to its high hardness, impressive tensile strength and a distinct thermal expansion coefficient is frequently used as a reinforcing phase in the hybrid composites [14].

Generally, the production routs of metal matrix nanocomposites can be divided into four different processes including liquid state, solid state, semi-solid-state methods and vapor deposition approaches [15]. The liquid-state processing of particulate reinforced composites is accompanied with some major disadvantages such as inadequate wettability between reinforcement and matrix, inhomogeneous distribution of the reinforcing particles in the matrix alloy and formation of brittle intermetallic compounds at the reinforcement/matrix interface. In order to tackle these significant drawbacks, powder metallurgy (P/M), as a simple cost-effective solid-state method, can be utilized to fabricate the near net shaped AMCs with a homogeneous distribution of reinforcement within the matrix alloys [16]. Recently, a novel high-efficiency P/M strategy called flake powder metallurgy (FPM) is used for processing of AMCs that utilizes flake-shaped metallic powders. This method could benefit more uniform distribution of reinforcements in the

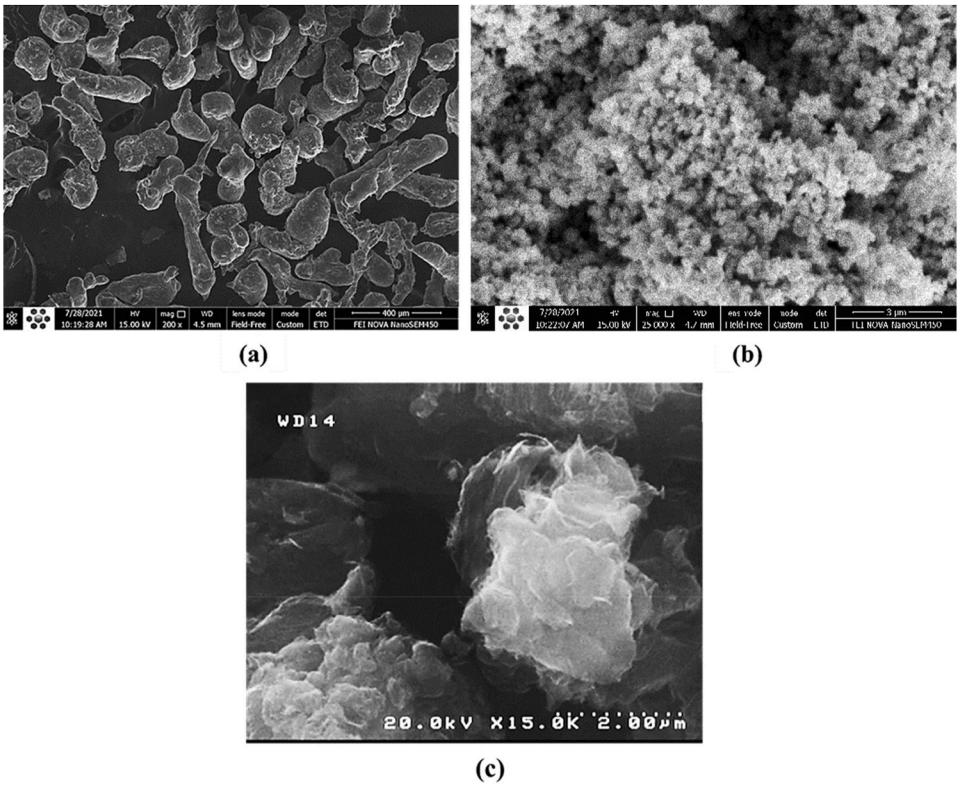

Fig. 2. FESEM micrographs of as-received powders; a) Al, b) WC and c) GNSs.

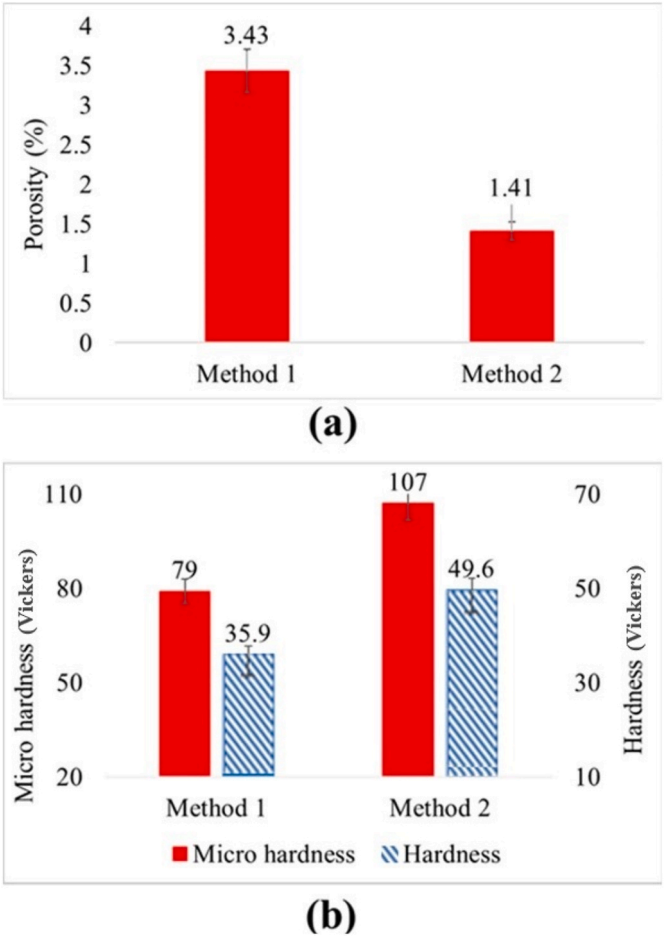

Fig. 3. a) Porosity and b) hardness and micro hardness of hot-pressed Al-0.1 vol% WC- 0.5 vol% GNSs fabricated by two different methods.

matrix resulting in improved strength and ductility [17,18]. Flake shaped particles also form a better interfacial bonding to graphene [19].

A survey of the current literature indicates that numerous experimental and simulation works have focused on development of Al matrix hybrid composites (AMHCs). Among the most studied AMHCs, those containing ceramic nanoparticles and graphene nanoplatelets, Al–SiC-GNPs, Al–TiC-GNPs, Al–B_4C-GNPs and Al–Al_2O_3-GNPs have been extensively explored exhibiting superior mechanical and wear properties [20–23]. In this context, Zheng et al. [24] investigated the effect of 0.25 wt% of SiC nanoparticles and different amounts of GNSs addition on the microstructure, hardness and tribological properties of hot-pressed Al7075 matrix nanocomposites. They reported that these hybrid nanocomposites exhibited higher hardness and wear resistance together with a lower coefficient of friction (COF) value as compared with Al–SiC nanocomposite and unreinforced matrix. In another report, Lin et al. [22] utilized a P/M method to fabricate Al2024–TiC-GNSs hybrid nanocomposites by using nano sized TiC particles and GNSs. They reported better dispersion of reinforcing nanoparticles in the matrix, leading to the greater hardness compared to the unreinforced Al matrix as well as a significant improvement in the wear resistance of the AMHC compared to the Al matrix alloy, Shafqat et al. [25] studied the mechanical, tribological, and electrochemical behaviors of Al6061–B_4C–GNSs matrix hybrid nanocomposites. They found that addition of B_4C and GNSs resulted in improved mechanical and wear properties of AMHCs. The Al-10 wt% B_4C-0.6 wt% GNSs nanocomposite exhibited superior hardness and compressive strength values, as well as low wear rate and COF values. However, further increase of GNSs from 0.6 to 1.2 wt%, resulted in a drop in the mechanical properties and wear performances. Applying the same approach, Şenel et al. [26] investigated the effect of Al_2O_3 and GNSs addition on the microstructure, physical and mechanical properties of Al–Al_2O_3-GNSs hybrid nanocomposites. They concluded that increasing the graphene content up to 0.1 wt% led to enhancement in the Vickers hardness and ultimate compressive strength of AMHCs. Samples contained more amount of graphene showed inferior mechanical properties due to the agglomeration and clustering of the GNSs. Zhang et al. [6] reported improved tensile strength and ductility of Graphene/ZrO_2/aluminum hybrid composite as compared with samples reinforced with either of graphene or ZrO_2 particles.

In recent years, a growing number of studies have been conducted to synthesize AMHCs reinforced with ceramic nanoparticles and GNSs by using different P/M methods [27]. Some approaches comprise a 2 step

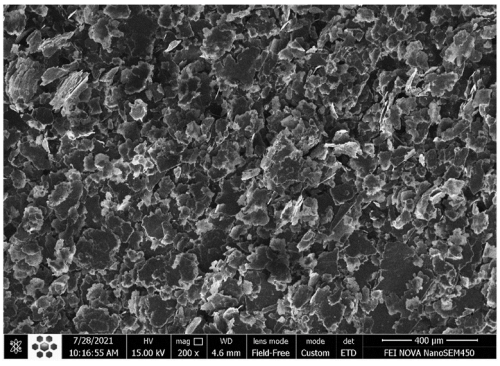

Fig. 5. FESEM photograph of 6h milled Al powders.

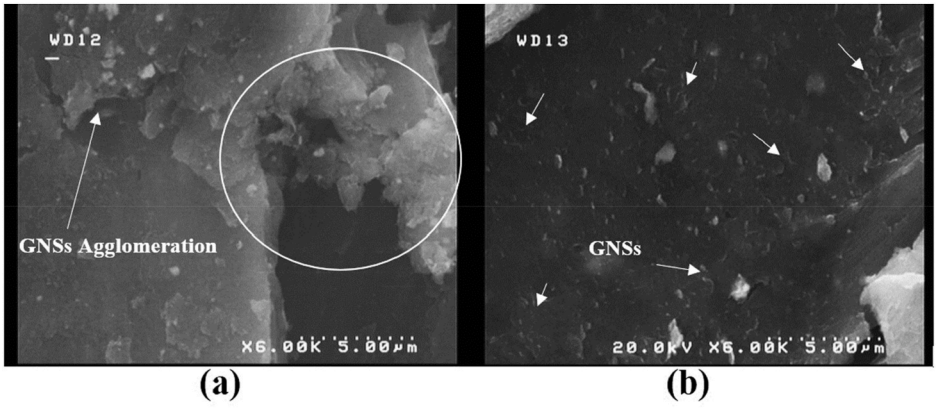

Fig. 4. FESEM images of powder samples fabricated by a) method 1 and b) method 2. Arrows indicate agglomerated GNSs.

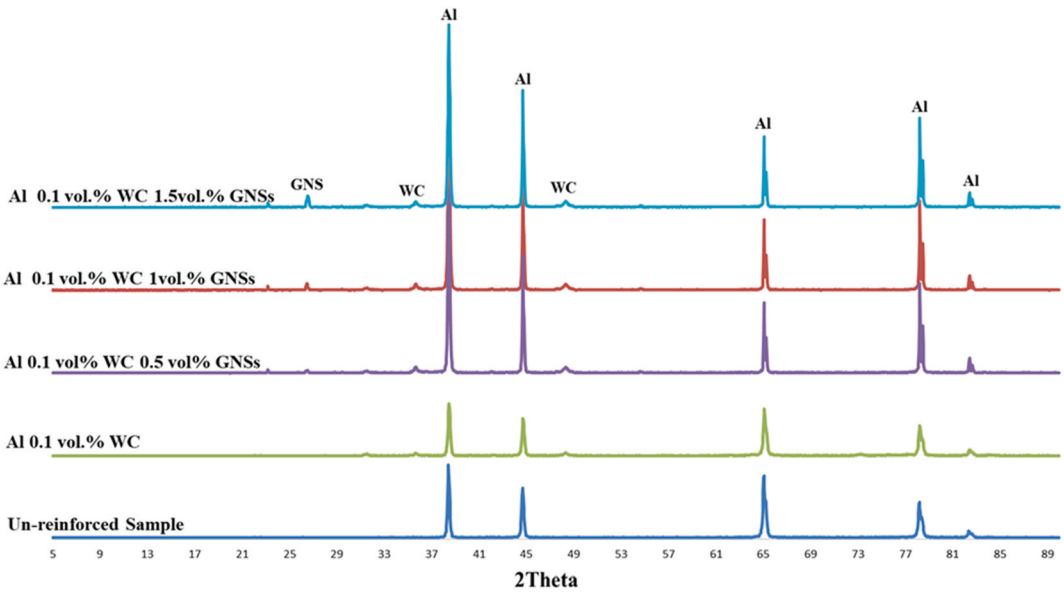

Fig. 6. XRD patterns of consolidated samples.

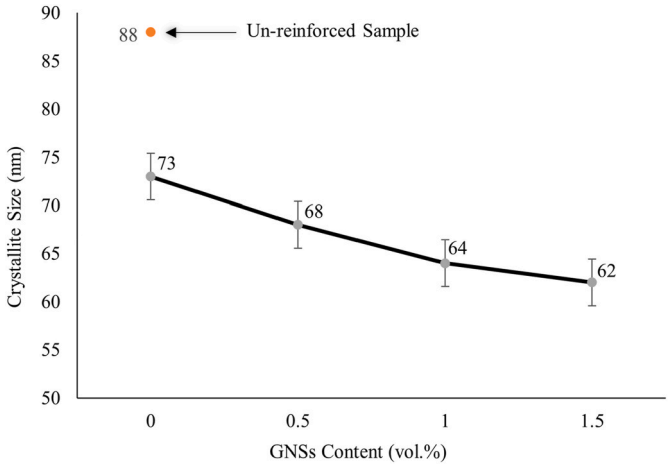

Fig. 7. The variation of crystallite size of consolidated Al- 0.1 vol% WC composites with their GNSs content. The data for the un-reinforced Al (reference sample) is also shown.

procedure involving ball milling the aluminum and ceramic particles and then mixing the composite powder with the graphene [28]. An alternative approach includes co-ball milling of aluminum, and ceramic reinforcing particles simultaneously in a single step [28,29]. However, according to the literature, there have been limited studies conducted to evaluate the mechanical properties of AMHNCs produced by using FPM. Above all, to the best of our knowledge, no research attempt has been devoted for exploring the microstructure, hardness and tribological properties of Al-WC-GNSs hybrid nanocomposite fabricated by FPM.

In this study, two different milling procedures assessed for optimizing the milling protocol. Furthermore, for the first time, through SEM studies of the tribo-layer morphology created on the wearing surfaces and other properties of the produced samples, the optimal amounts of GNSs and WC nanoparticles for enhanced performance of Al-WC-GNSs hybrid nanocomposites prepared via FPM and hot pressing investigated.

2. Materials and methods

2.1. Materials

Commercially pure gas atomized Al (125–180 μm, D_{50} = 166.5 μm) with 99.5 % purity), WC nano-particles (US Research Nanomaterial Inc with an average size of 50 nm) and GNSs (United Nanotech Innovations, specific surface area ≥330 m^2/g, thickness = 1–2 nm, plate width ≤1 μm with 98 % purity) are used to fabricate Al/WC/GNSs hybrid nanocomposites. The nominal chemical composition and the size distribution of Al particles determined by laser particles size analyzer (LPSA, model CILAS, France) can be seen in Table 1 and Fig. 1, respectively. Fig. 2a to c illustrate the field scanning electron microscope (FESEM) images of Al, WC particles and graphene sheets.

2.2. Composite preparation

Al-WC-GNSs nanocomposites were produced by FPM utilizing a PM-2400 planetary ball mill under a 5-bar argon atmosphere. The rotational speed of 300 rpm, a ball-to-powder ratio of 15:1, 2–5 mm sized wear-resistant steel balls and 6 or 8 h milling times were selected as the milling parameters. In order to prevent adhesion of aluminum powders to the balls, 1.5 wt% of stearic acid was also used as the Process Control Agent (PCA). The milled powders were consolidated in a steel die with an inner diameter of 29 mm and height of 100 mm by hot pressing at 380 °C by applying 750 MPa pressure for 8 min.

In order to optimize the mixing method of reinforcements and aluminum, the following methods were evaluated.

1 Al and WC powders were mixed, and ball milled for 6h, followed by adding GNSs to the mixture and milling for another 2h.
2 A mixture of Al, WC and GNSs powders ball milled for 6h.

Our previous study [30] discussed a procedure of creating a layered structure in the final products. To accomplish this, a glass tube was positioned on the steel die cavity and the milled flake powders were allowed to settle in the mold cavity on their largest surface after travelling along the mold height. This provided improved alignment and distribution of Al flakes, which in turn enhanced the mechanical properties of the final product.

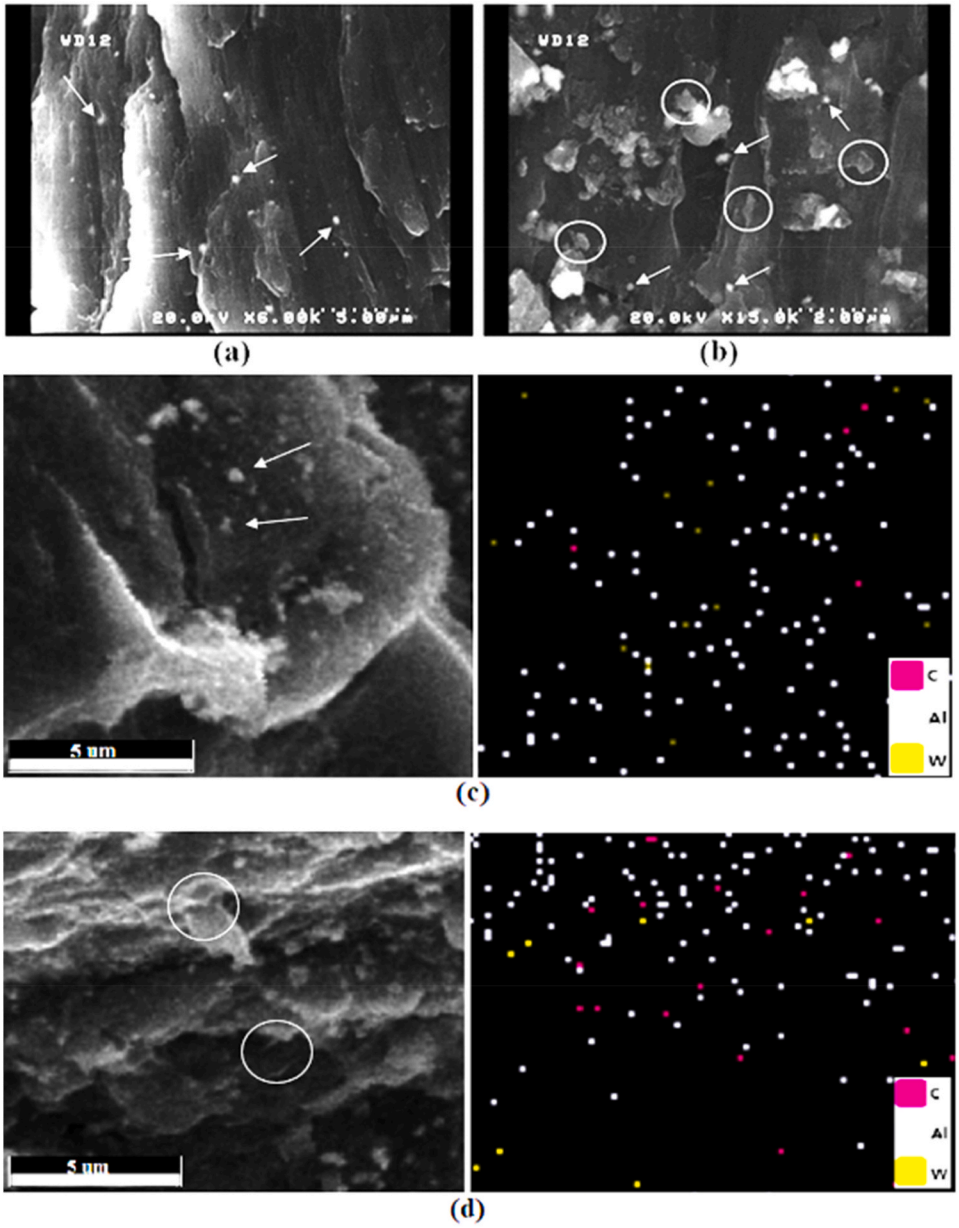

Fig. 8. Typical FESEM and EDAX images of the cross sectioned (a, c): Al-0.1 vol% WC and (b, d): Al-0.1 vol% WC-0.5 vol% GNSs samples. Arrows represent WC clusters and circles show GNSs.

2.3. Characterization of samples

Structural characterization of the as-milled powder and consolidated samples were performed by means of X-ray diffraction (XRD) analysis with Cu-Ka radiation ($\lambda = 1.5406$ Å) in the range of $2\theta = 5^\circ$ to 85°. The Debye-Scherrer's method was used to measure the crystallite size of aluminum using the following equation:

$$D = K\lambda / \beta Cos\Theta \quad (1)$$

where D represents the crystallite size, K is the shape factor (equal to 0.89), λ is the wavelength of Cu Kα (equal to 1.5406 Å), β is the full width of half maximum peak (FWHM) and Θ is the position of the peak. The FWHM was measured from the XRD patterns after subtracting the Cu Kα2 sub-peaks and applying an instrument error of 14 %. This was done using the following equation:

$$\beta^2_{real} + \beta^2_{instrument} = \beta^2_{measured} \quad (2)$$

The optical microscope (OPYMPUS BH2-UMA, USA) and field emission scanning electron microscope (FESEM, model FEI Nova NanoSEM 450) utilized for microstructural characterization of the etched surfaces of the consolidated specimens and the cross-sections of the samples, respectively. Keller's solution composed of HCl, HF, HNO3, and H_3PO_4 was used as an etchant for the microstructural characterization of the consolidated nanocomposites. The relative density and porosity of nanocomposites were determined according to the ratio of measured density quantified by the Archimedes' principle and theoretical one calculated by rule of mixture as follows:

$$\rho_c = \rho_m V_m + \rho_r V_r \quad (3)$$

where ρ and V respectively represent the volume fraction, and density while c, m and r denote composite, matrix, and reinforcement respectively. The microhardness of the samples was measured on a Vickers microhardness tester (Wolpert, Germany) at a load of 30 g with a dwell time of 10 s. The mean value of 5 hardness measurements conducted on

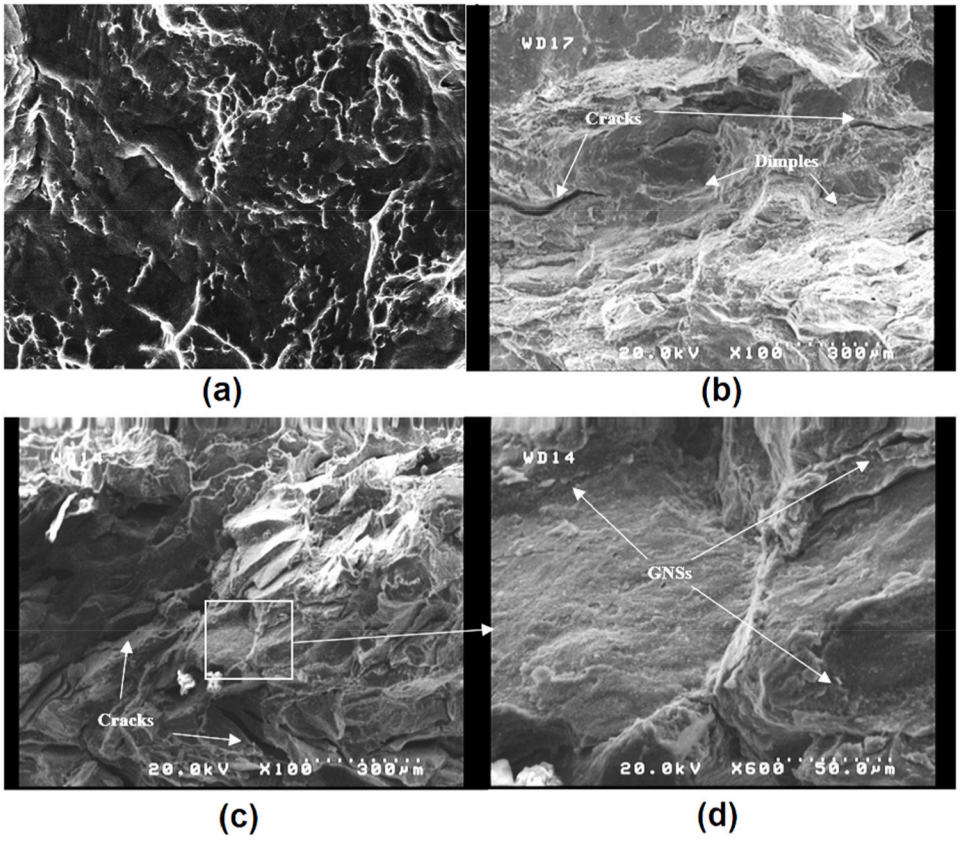

Fig. 9. Fractured surfaces of (a) reference sample, (b) Al- 0.1 vol% WC composites, (c and d) Al- 0.1 vol% WC, 1 vol% GNSs composite.

each sample was considered. In addition, macro hardness of the samples was quantified by applying a load of 50 N for 10 s using an automatic Vickers hardness tester (Inovatest, Netherlands). The mean value obtained from 10 measurements was reported for each sample.

The tribological behavior of the samples was studied using a pin-on-disk setup according to the ASTM G-99 standard test method. A 52100 steel pin with 64 Rockwell hardness was used as the counterpart for each wear testing. The wear tests were conducted at room temperature at loads of 3, 5 and 7 N (0.15, 0.25 and 0.35 MPa) with a speed of 0.3 m/s. The sliding distance and diameter of the wear track were 750 m and 8.5 mm respectively. For determining the coefficient of friction (COF), data obtained for the initial distance of wear testing was excluded. The average value of COF quantified for final 100 m of wearing was considered.

3. Results and discussions

3.1. Ball milling procedure

Fig. 3a and b indicate the porosity, hardness and microhardness of hybrid composites containing 0.5 vol% GNSs fabricated by the two various milling methods. As can be seen, the sample fabricated by the second method exhibited reduced porosity as well as higher micro and macro hardness values. Fig. 4 shows the FESEM images of the milled powder mixtures obtained through the first and second milling methods. The agglomerated GNSs in the sample produced with the first method are clearly seen in Fig. 4-a. On the other hand, the sample produced via the second method exhibits a more uniform and evenly distributed GNSs within the powder mixture.

The uniform distribution of GNSs in the matrix alloy obtained via the first method resulted in decreased porosity and increased hardness values. Consequently, the first method of ball milling was utilized to fabricate the composite samples for further studies as reported in this study.

The FESEM image of the Al powders milled for 6 h as shown in Fig. 5 confirms severe plastic deformation imposed on the ductile Al particles. The morphology of powders has changed from semi-spherical (Fig. 2a) to flake-shaped.

Consolidated samples fabricated by using flake-shaped aluminum particles resulted in the formation of a distinctive layered structure, as a common characteristic feature of FPM products can result in several advantages such as being more geometrically compatible with the nano-sized reinforcements [31].

3.2. X-ray diffraction

The XRD patterns of the consolidated reference sample and samples containing 0.1 vol% of WC nanoparticles together with 0, 0.5 and 1.5 vol % of GNSs are shown in Fig. 6.

As shown, the absence of carbides or oxides in these patterns confirms that the temperature used in the fabrication process (450 °C) was insufficient for formation of such unwanted phases.

The variation of crystallite size of consolidated samples with their GNSs content is shown in Fig. 7. It can be seen that 0.1 vol% addition of WC nanoparticles to unreinforced Al matrix (reference sample) caused 17 % reduction in crystallite size. According to previous studies [32,33], ball milling of metallic materials results in decreased crystallite size due to induced plastic deformation [34]. On the other hand, in agreement with another report [35,36] the presence of hard particles in powder mixture intensifies the plastic deformation during the milling process leading to further decrease in crystallite size. This is the primary reason for obtaining smaller crystallite size for Al-0.1 vol% WC as compared to that of the reference sample. The decreased crystallite size of composites with their increased GNSs content is attributed to the presence and increased amount of GNSs contributing in increased plastic deformation imposed on Al matrix during milling. Varol et al. [37] stated that

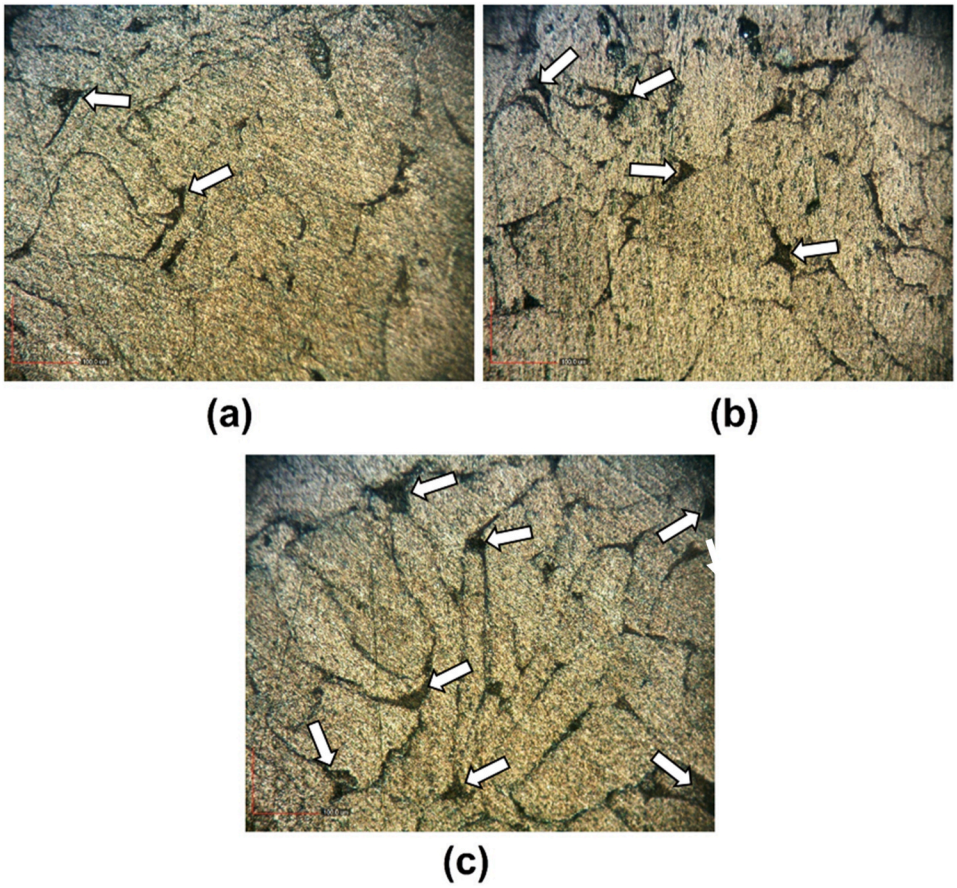

Fig. 10. Optical images of sample (a) reference sample, (b); Al- 0.1 vol% WC and c) Al- 0.1 vol% WC 1 vol% GNSs composites. Arrows indicate pores.

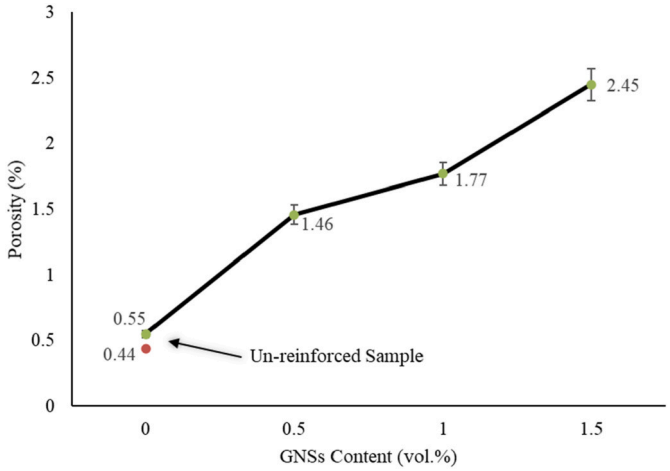

Fig. 11. The variation of the porosity of Al- 0.1 vol% WC-GNSs hybrid composites with their GNSs content. The porosity of the unreinforced sample is also shown.

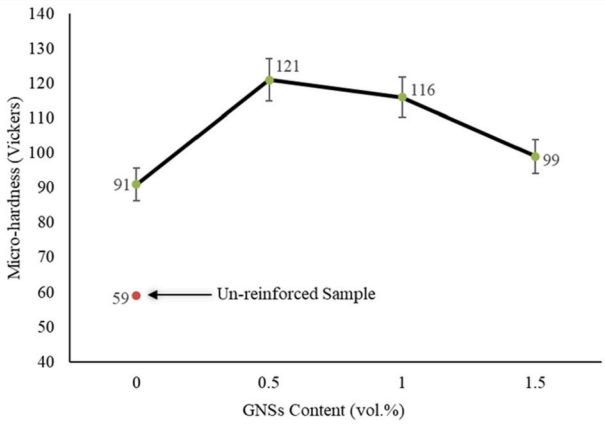

Fig. 12. The variation of Vickers microhardness of Al- 0.1 vol% WC-GNSs hybrid composites with their GNSs content. The microhardness of the unreinforced sample is also shown.

co-milling of copper with multilayer graphene reinforcement for 5 h resulted in decreased crystallite size of the matrix. They attributed it to the presence of reinforcement nanoparticles in the powder mixture. However, they found that the addition of hard WC particles had more influence on the crystallite size of the matrix as compared with GNSs addition. It is noted that GNSs, whether located on the particles surfaces or dispersed within the particles, affected the dislocation movements [38]. Furthermore, the planar morphology of the GNSs combined with a high specific surface, provided an additional barrier against the dislocation movements [39].

3.3. Microstructure

Typical FESEM and EDAX images of the cross sectioned Al-0.1 vol% WC nanocomposite and Al-0.1 vol% WC-0.5 vol% GNSs hybrid sample as respectively presented in Fig. 8 a and b, confirm the uniform distribution of reinforcements in the nanocomposites. In agreement with another report [40], the GNSs, WC nanoparticles and WC clusters not

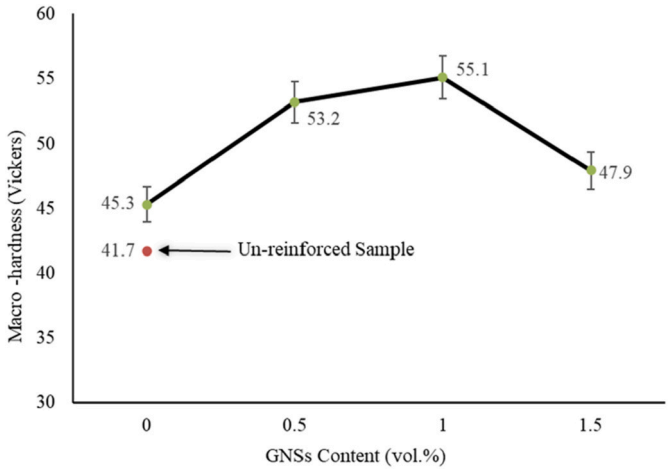

Fig. 13. The variation of Vickers macro hardness of Al- 0.1 vol% WC-GNSs hybrid composites with their GNSs content. The macrohardness of the unreinforced sample is also shown.

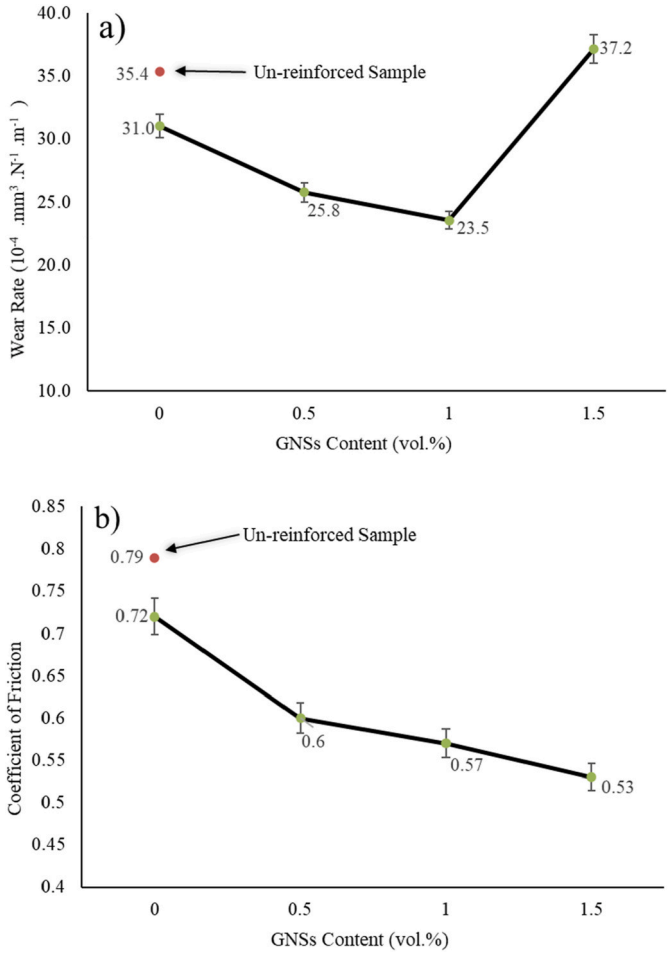

Fig. 14. The variation a) Wear rate and b) COF of Al- 0.1 vol% WC-GNSs hybrid composites with their GNSs content. The values for the unreinforced sample are also shown. The load and sliding distance were 7 N and 500 m respectively.

only located on the individual Al particle surfaces, but also penetrated into them.

Fig. 9 a-d show the FESEM images of fractured surfaces of the

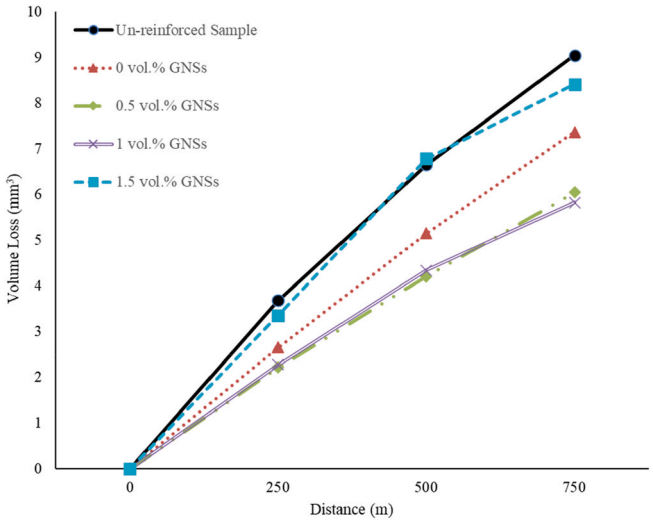

Fig. 15. The variation of volume loss with sliding distance for different samples under the applied normal load of 5 N.

Table 2
The wear rate in 3 intervals of wearing distance under the applied load of 5 N for Al- 0.1 vol% WC-GNSs hybrid composites with different GNSs contents. The value for the unreinforced sample is also shown.

Composite GNSs content (vol%)	Wear Rate (10^{-3} $mm^3.m^{-1}$)		
	0–250 m	250–500 m	500–750 m
Un-reinforced Sample	14.7	11.9	9.6
0	10.6	10	8.9
0.5	8.8	8	7.3
1	9.1	8.9	7.3
1.5	13.4	13.7	6.5

reference sample and hybrid composites containing 0.1 vol% of WC together with 0 and 1 vol% of GNSs. It has been speculated that agglomerated reinforcements act as nucleation sites during fracturing, forming disfigurements and dimples on the images of the fractured surfaces [41]. This phenomenon is represented in Fig. 9-b of Al- 0.1 vol% WC composite, exhibiting a mixed ductile-brittle fracture behavior with a rough surface and multiple ductile dimples. This microstructure is opposed to the smooth surface and ductile fracture behavior of the unreinforced reference sample shown in Fig. 9-a. The fine cracks as well as the reduced number of ductile dimples observed on the fractured surface of the hybrid nanocomposite (Fig. 9-c,d), indicate a change in the failure mechanism to a more brittle fracturing. Cracks in aluminum composites containing 1 % graphene as observed in another report [42], indicates the reduced ductility as compared to Al- 0.1 vol% WC composite. Moreover, as previously reported, reinforced composites exhibiting higher hardness often demonstrate a more brittle fracture surface [43], which is consistent with the findings of the present study.

3.4. Porosity

Fig. 10 a-c show the optical micrographs of the etched surfaces of the consolidated specimens. The percentage of porosity shows a rising trend with the increased reinforcement content. These results are in agreement with several previously reported findings [17,44,45].

The variation of the porosity of Al-0.1 vol% WC-GNSs hybrid composites with their GNSs content as shown in Fig. 11 indicates that addition of 0.1 vol% of WC nanoparticles to the matrix (unreinforced sample) resulted in 0.11 % rise in porosity. Moreover, the porosity of hybrid nanocomposites increased with their GNSs content. These results in agreement with Fig. 10 attributable to the presence and increased

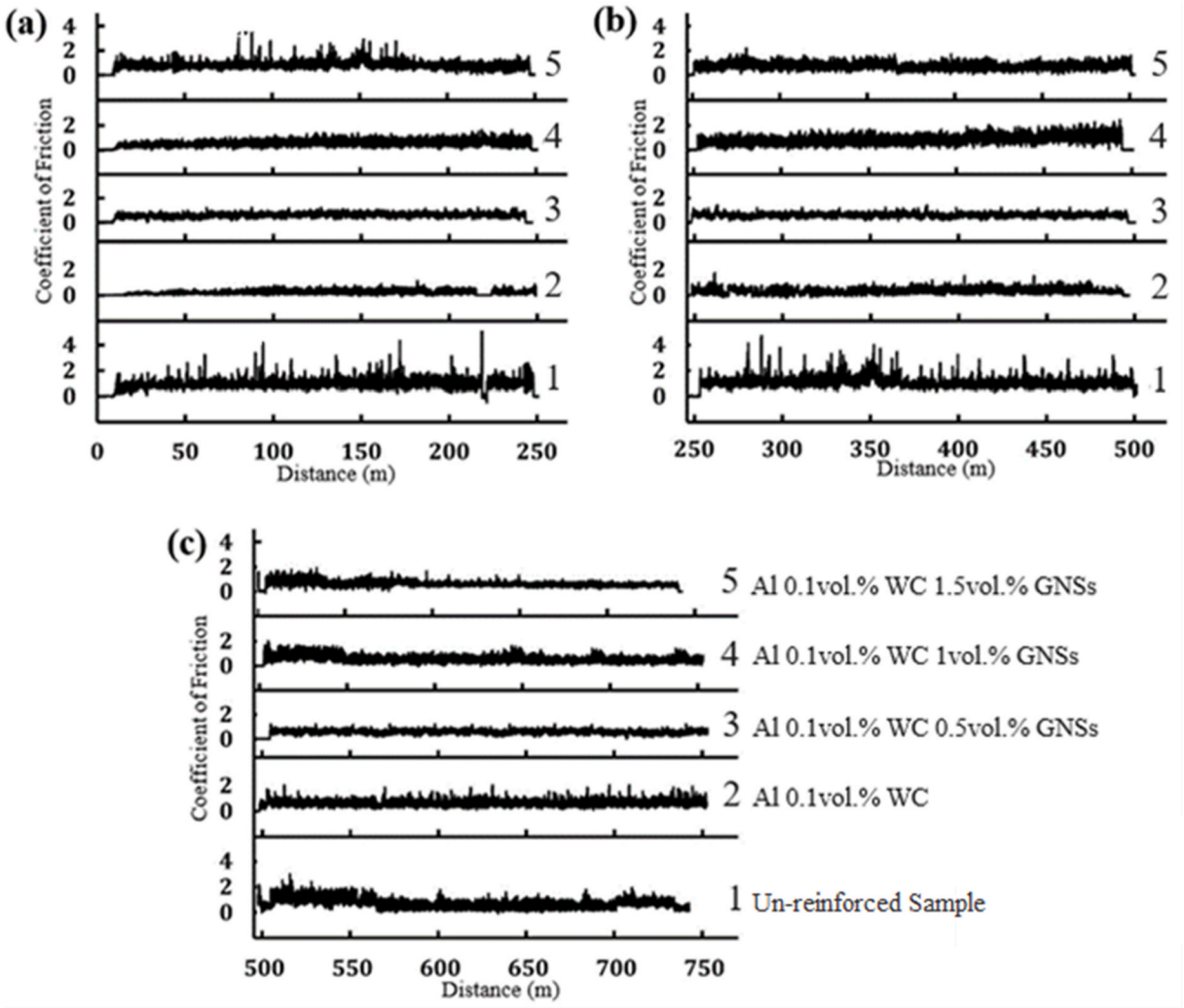

Fig. 16. The variation of the COF under 5 N load for various samples during three sliding distance intervals of: a) 0–250 m and b) 250–500 m c) 500–750 m.

content of hard and non-deformable reinforcements such as WC and GNSs. These particles inhibited effective densification of samples during hot-pressing. In addition, these hard particles served as supplementary milling media during milling resulting in intensified strain [22], reduced crystallite size of the matrix (Fig. 7) and increased hardness of the matrix alloy, all contributing in inferior densification during compaction of powders.

3.5. Hardness

The variation of the micro-hardness and macro-hardness of Al- 0.1 vol% WC-GNSs hybrid composites with their GNSs content are shown in Figs. 12 and 13 respectively. According to these Figs. addition of 0.1 vol % of WC to the unreinforced (reference) sample leads to an increase of 54 % and 9 % in its microhardnesss and macroharsness values. It is also clear that the hardness values experienced respectievly another 33 % and 17 % growth for micro and macro-hardness by addition of 0.5 vol% GNS. The increased hardness of hybrid nanocomposites continued by addition of 1 vol% of GNSs but dropped for 1.5 vol% addition of these particles. However, maximum micro-hardness obtained for Al–1%WC-0.5 % GNSs composite and decreased by further increased GNSs. The increased hardness values is attributed to several parameters. Grain refinment (Hall-Petch), Orowan and thermal mismatch are three main strengthening mechanisms in aluminum matrix nano-composites [46–48]. Also uniform distribution of hard reinforcing particles within the matrix alloy as well as strong interfacial bonding between reinfocements and matrix enhance mechanical properties of composites [49]. The uniform distribution of hard WC nanoparticles and GNSs in the Al matrix obtained via the FPM process contributed in restricted motion of dislocations [50]. The grain boundary motion is restricted by the reinforcement particles. The presence of these hard reinforcing particles also allows for the triggering of the Orowan mechanism [51]. The reinforcing particles can constrain grain growth during hot pressing and contribute to strengthening of composites via the Hall-Petch mechanisem. Lastly, significant difference in the coefficient of thermal expansion coefficient values of the used reinforcements and aluminum [50–52] contributed to the increased density of dislocations within the composite samples.

The decreased microhardness of the hybrid composite samples by further increased GNSs content from 0.5 to 1.5 vol% (Fig. 12) can be attributed to deterioration in the uoniformity of GNSs distribution in the Al matrix caused by agglomeration and clustering of these particles. Weak bonding between particles in clusters and between aglomerated particles and matrix alloy causes inferior mechanical properties [52]. The same trend has been reported for Al-Graphene oxide composites [53].

According to Figs. 10 and 11, both the addition of WC nanoparticles and increased GNSs content resulted in increased porosity of samples. Obviously the increased porosity results in decreased macrohardness of samples [54]. Howerver, the positive effect of addition of up to 1 vol% of

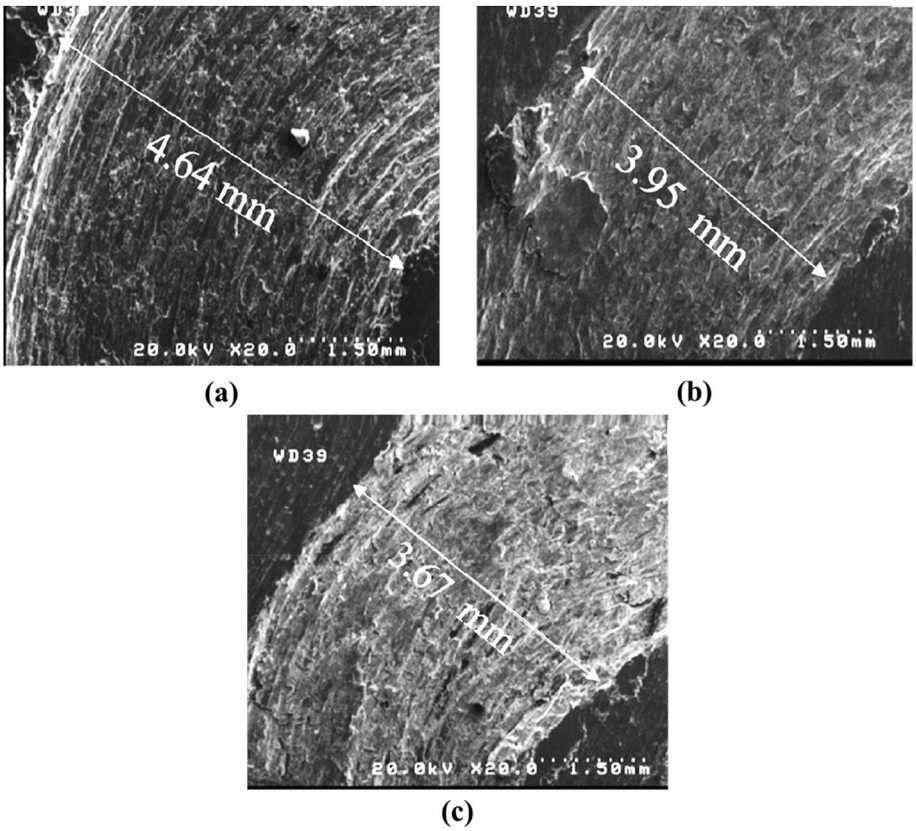

Fig. 17. The SEM micrographs of wear track of a) the un-reinforced sample, b) Al-0.1 vol% WC nanocomposite and c) Al-0.1 vol% WC-1 vol% GNSs hybrid nanocomposite.

GNSs in enhancing hardness of composites, as discussed before, compensated the negative effect of porosity resulting in increased hardness as shown in Fig. 13. Nevertheless, the deleterious effect of porosity in the composite contained more than 1 vol% of GNSs dominated positive effects of GNSs addition resulting in decreased hardness of the composite. These results are in agreement with previously reported findings for hardness of nanocomposites that declined with more than 1 vol%. GNSs addition [40].

3.6. Wear

3.6.1. Effect of GNSs content

Fig. 14 (a, b) indicate wear rate and coefficient of friction values of un-reinforced sample, Al-0.1WC nano-composite and Al-0.1WC-GNSs hybrid nanocomposites with different GNSs contents. As seen, addition of 0.1 vol% WC caused a 13 % reduction in the wear rate of non-reinforced sample. It is also clear that addition of up to 1 vol% GNSs to Al- 0.1 vol% WC composite resulted in decreased wear rate, so that the hybrid nanocomposite containing 1 vol% GNS exhibited the minimum wear rate within the investigated samples being 34 % lower than that of the un-reinforced sample. However, by increasing the GNSs content from 1 to 1.5 vol% the wear rate of hybrid nanocomposites experienced an ascending trend. Such behavior can be exactly correlated with hardness values as shown in Fig. 13.

The correlation between the wear resistance of materials and their hardness is well-established based on the Archard equation (Eq. 4), which is supported by numerous research reports [4,55,56].

$$Q = \frac{K^{*}W^{*}L}{H} \tag{4}$$

where Q denotes the volume of the worn material, K is a dimensionless constant, W is the normal applied load during wearing test and L and H respectively represent the sliding distance and the hardness of the sample.

The ascending trend observed in wear rate of composites is due to the reduction in their hardness and strength via the deteriorating effects of GNSs agglomeration and increased porosity. These agglomerated particles, due to weak bonding with the matrix, could be easily detached from the wearing surface and increase the wear rate.

Fig. 14 indicates that addition of reinforcements results in a continuous decrease in the coefficient of friction (COF). This downward trend has been also reported in previous studies [57,58] and can be caused by three main reasons.

1 Increasing the hardness and micro hardness by addition of reinforcements which can lead to lower COF values [59].
2 Interlayer sliding due to weak Van der Waals bond between graphene sheets [60].
3 Lubricating effects of the graphene sheets providing a tribolayer on the wearing surface [55].

It is also worth mentioning that despite the decreased hardness of the hybrid composite by addition of 1.5 % GNSs, due to more GNSs that are available on the wearing surface, the coefficient of friction decreased.

Another significant reason for improving the tribological properties of hybrid nanocomposites compared to those of the monolithic sample or the Al-0.1 vol% WC nanocomposite is the increased conductivity of these materials. In fact the relatively high thermal conductivity of graphene [28,42] reduce the softening of wearing surface caused by temperature rise during wearing test leading. This effect in turn decreases the amount of detached debris from the surface and results in lower coefficient of friction [56].

In order to gain a deeper understanding of the effect of reinforcing particles on the wearing mechanisms of composites, the changes of the

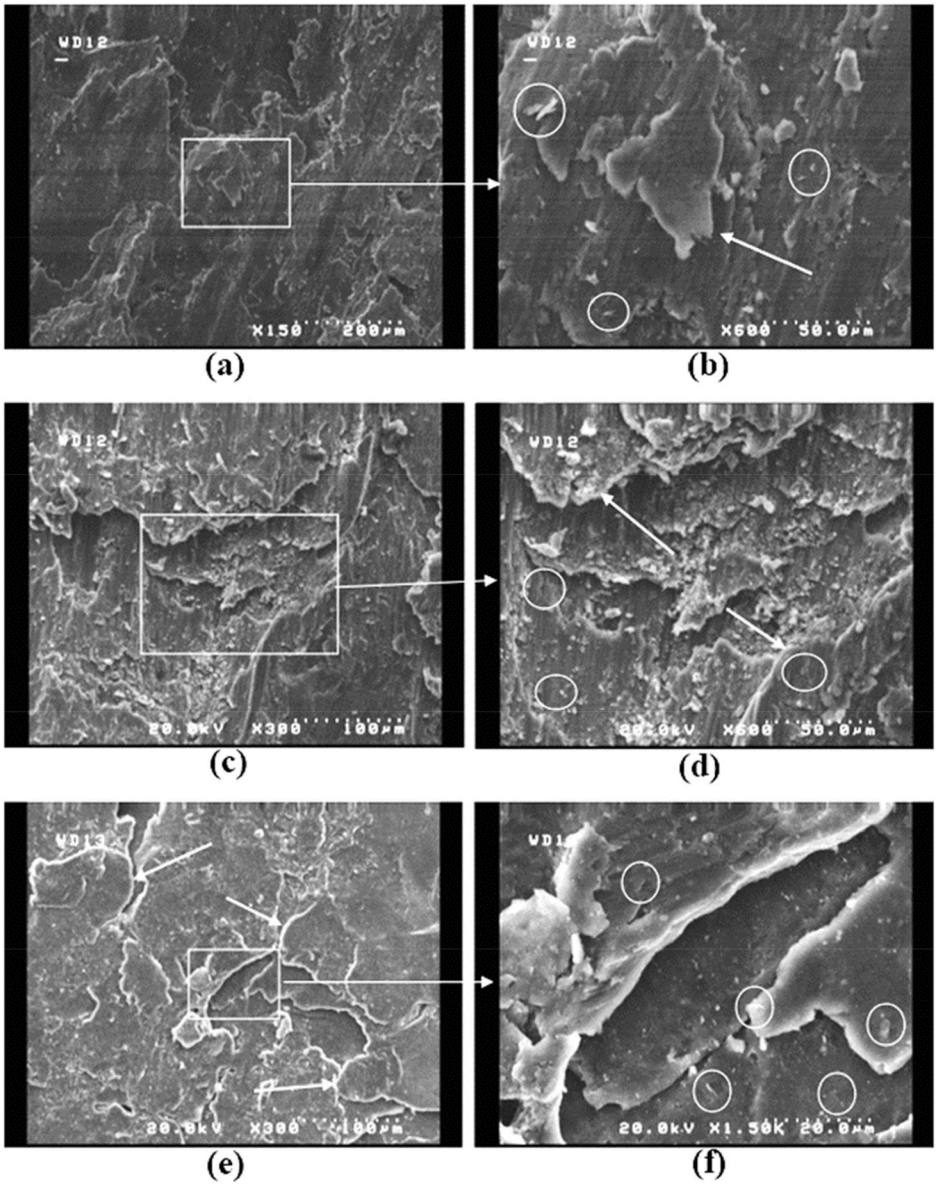

Fig. 18. FESEM images of the worn surface of the sample containing 1 vol% GNSs taken at different sliding distance intervals of 250 (a and b), 500 (c and d), and 750 m (e and f) during the wearing test performed under 5 N load. Arrows indicate the formed tribo-films and circles show GNSs on the wearing surface.

volume loss at different wearing distances and under different loads investigated. The variation of the volume loss of different samples under 5 N load with sliding distance are illustrated in Fig. 15. Each line corresponding to a sample represent three different slopes for three sliding distance intervals. The slopes are the volume wear rate values as tabulated in Table 2 confirm that the wear rate for composites, particularly hybrid composites, decreases with increased sliding distance.

The sample containing 1.5 vol% of GNSs, showed a high slope between second and third stages (500 m–750 m) which reveals the perfect formation of tribo-films on the wearing surface. As previously reported, GNSs act as diffusion barriers and prevent oxygen diffusion through grain boundaries which takes place at higher temperatures. This phenomenon prevents formation of brittle oxide phases at grain boundaries causing the reduced wear rate [61,62].

The variation of the COF under 5 N load for various samples during three sliding distance intervals are shown in Fig. 16. The COF values obtained for the un-reinforced sample is generally higher than those of its composite counterparts and represent large fluctuations. Hybrid composites display more stable diagrams except for the composite containing 1.5 vol% GNSs. The increased COF fluctuation observed in the composite containing 1.5 vol% GNSs is probably related to its higher porosity. Similar result has been reported in a study of hybrid metal matrix composites [63] In addition, as evidenced by Table 2 and Fig. 16, the COF decreases with increased sliding distance, exhibiting the lowest COF values for the last wearing distance interval. Table 2 demonstrates a substantial 48 % reduction in the COF for the composite with 1.5 vol% GNSs in the final wearing distance interval as compared to the initial interval. These results can be attributed to the increased amount of GNSs transferred to the wearing surface with increased sliding distance. Additionally, temperature rise during the wearing test causes a micro-thermal softening. This effect results in reduced bonding strength between the matrix and reinforcements that enhances the GNSs pull out from matrix [64]. The pulled out GNSs reduce the COF by forming rollers [55] and layer buckling resulting in interlayer sliding due to weak interlayer bonding of GNSs [65].

These findings suggest that at longer wearing distances, due to increased amount of pulled out GNSs and formation of a relatively thick tribo-layer on the wearing surface, a change in wearing mechanisms

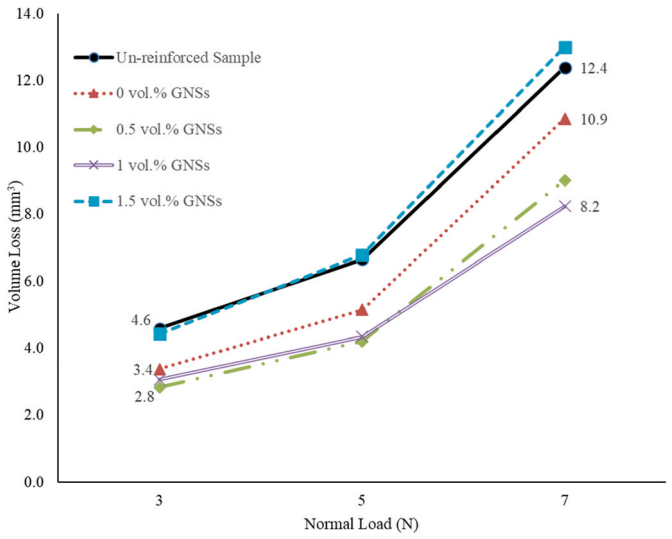

Fig. 19. The variation with the applied load of the volume loss of Al-0.1 vol% WC composites containing different amounts of GNSs quantified after 500 m sliding distance. The data for the un-reinforced sample is also presented for comparison.

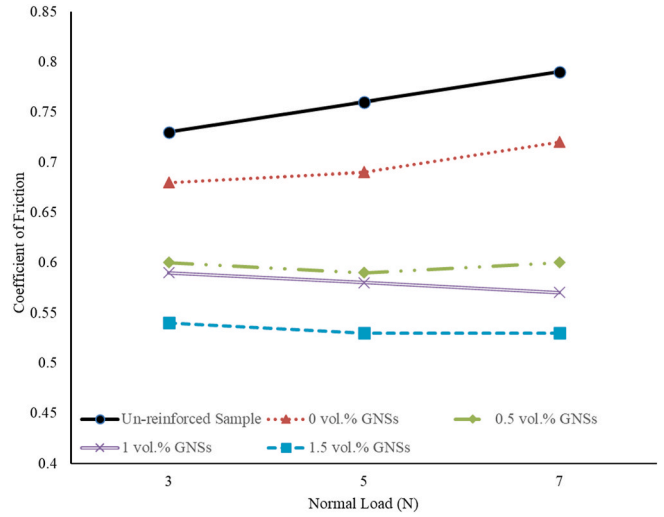

Fig. 20. The variation with the applied load of the COF of Al-0.1 vol% WC composites containing different amounts of GNSs quantified for the last 100 m of wear distance. The data for the un-reinforced sample (reference sample) is also presented for comparison.

occurred. Subsequently, this could lead to decreased COF and a lower wear rate especially in the final stage of wearing test as shown in Fig. 16-c [66,67].

Fig. 17 a-c represent the SEM micrographs of wear track of the un-reinforced sample, Al-0.1 vol% WC nanocomposite and Al-0.1 vol% WC-1 vol% GNSs hybrid nanocomposite to be considered for investigating the wear mechanisms of different samples. As can be clearly seen, the width of wear track of the hybrid nanocomposite is smaller than that both of the Al-0.1 vol% WC nanocomposite and un-reinforced sample indicating the enhancement of the wear resistance in the nanocomposite specimen.

Fig. 18 shows a series of FESEM images of the worn surfaces of a hybrid sample containing 1 vol% of GNSs taken at three different sliding distance intervals. Fig. 18-a and 18-b, which depict the first stage of wear (first 250 m), show that the material weak point is at particle boundaries and GNSs agglomerated zones. Grooves, as indicated in these Figs. indicate the formation of insufficient tribolayer at this stage. During the second stage of wear (250–500 m), numerous small wear debris particles covered by GNSs were observed. The tribo-film seemed to form and expand on the wearing surface while deep grooves were visible in the spaces between the developed tribo-films. Additionally, higher concentrations of graphene-rich wear debris were detected in the grooves, which may be a consequence of material transformation from the underneath surface due to the weak bonding of GNSs and the matrix alloy [66,67]. In the third stage (500–750 m), the surface had become smooth and was covered with the tribo-film, with a lower number of detected wear debris. This implies that the wear process had entered a steady state, resulting in a lower volume loss.

In agreement with our previous study [30], the dominant wear mechanism of the un-reinforced sample was adhesive wear while Al-0.1 vol% WC sample exhibited a mixed adhesive and abrasive wear mechanism. The bright region as shown in the SEM image of Fig. 17 c, indicates GNS-rich surface. The laminar surface morphology of the wear tracks as shown in Fig. 18 implies occurrence of extensive plastic deformation. According to Fig. 18, rough wear surface morphology with high plastic deformation and material flow observed at two initial distance intervals suggest adhesive wear mechanism. At the third stage, formation of a thick tribo-layer resulted in creation of a smooth wear surface. In this case, the presence of micro cracks and laminated morphology suggest a mixed adhesive-abrasive wear mechanism.

3.6.2. *Effect of applied load*

Fig. 19 shows the effect of applied load on the volume loss of Al-0.1 vol% WC composites containing different amounts of GNSs. As was expected, the increased applied load resulted in increased volume loss for all the investigated samples. However, this effect was more significant for the second loading interval as indicated by the sharp increase in the slopes of the corresponding lines. In addition, the deviation between the lines corresponding to all of the composites increased with increased applied load. For example, when the applied load was 3 N, the worn volume was almost equal for the composites containing 0, 0.5 and 1 vol % of GNSs. At 5 N load, the composite with no GNSs addition deviated from the two other composites and exhibited a higher volume loss value. At the applied load of 7 N, the volume loss in these composites entirely deviated from each other. These results can be attributed to formation and extension of the tribolayer on the wearing surface.

It is clear that the extraction of GNSs from the inner regions of samples requires a specific level of shear stress, which is intensified under elevated loads [68]. Therefore, the beneficial effect of GNSs addition in reducing the wearing volume loss through formation and completion of a tribolayer on the wearing surface was more evident at higher applied loads. It is interesting to note that the response to increased applied load of the hybrid composite containing 1.5 vol% of GNSs, was almost identical to that of the un-reinforced sample. For this sample the deteriorative effect of the high porosity (Fig. 12) dominanted over the beneficial effect of formation a complete tribolayer on the wearing surface.

The variation of the COF of different samples with the applied load during wearing test is shown in Fig. 20. For the samples with no GNPs addition, in agreement with previous reports [69,70], the increased applied load lead to higher COF. However, addition of GNSs to samples has changed this trend, so that in hybrid composites containing 1 and 1.5 vol% of GNSs there is an inverse relationship between the coefficient of friction and the applied load. This phenomenon can be elucidated by the increased tendency for formation a tribolayer on the wearing surface at higher applied shear stresses as was discussed before.

Furthermore, it is worth mentioning that the sample contained 1.5 vol % of GNSs exhibited the lowest COF values regardless of the magnitude of the applied load. In addition, the COF of this composite was nearly constant for all the applied loads. This means that for this hybrid composite even the applied 3 N load was enough for formation of a tribolayer covering the whole area of the wearing surface. However,

for the sample containing 1 vol% of GNSs, the development of the tribolayer enhanced with applied load implying that a certain amount of load was required for development of a complete tribolayer on the wearing surface.

4. Conclusions

This study presents a novel method for processing the Al-WC-graphene nanosheets (GNSs) hybrid nanocomposite via flake powder metallurgy. Milling of all the constituent powders for 6 h gave better results than milling of Al + WC for 6 h, followed by adding GNSs and continuing milling for 2 h. While higher GNSs content increased porosity, hardness improved by up to 1 vol% GNS addition. The enhanced hardness, along with the formation of a protective tribo-layer, resulted in improved wear resistance. Notably, the coefficient of friction (COF) decreased as hardness increased. These findings suggest that by optimizing the reinforcing particles contents and processing parameters the tribological performance of this promising hybrid nanocomposite can be tailored for various applications.

CRediT authorship contribution statement

Mohsen Saremi Ghareh Gol: Writing – original draft, Visualization, Investigation, Formal analysis. **Abolfazl Malti:** Writing – original draft, Visualization, Investigation, Formal analysis. **Farshad Akhlaghi:** Writing – review & editing, Supervision, Project administration, Conceptualization.

Declaration of competing interest

The authors declare that they have no known competing financial interests or personal relationships that could have appeared to influence the work reported in this paper.

Data availability

No data was used for the research described in the article.

References

[1] İ. Ovalı, et al., Mechanical properties of al2024/al2o3/mgo/graphite composites via hydro-thermal hot pressing route, Mater. Chem. Phys. 302 (2023) 127779, https://doi.org/10.1016/j.matchemphys.2023.127779.

[2] W.S. Barakat, et al., The effect of cu coated al2o3 particle content and densification methods on the microstructure and mechanical properties of al matrix composites, J. Mater. Res. Technol. 24 (2023) 6908, https://doi.org/10.1016/j.jmrt.2023.05.010.

[3] R. Balokhonov, V. Romanova, A. Kulkov, Microstructure-based analysis of deformation and fracture in metal-matrix composite materials, Eng. Fail. Anal. 110 (2020) 104412, https://doi.org/10.1016/j.engfailanal.2020.104412.

[4] S. Tang, et al., Microstructure and mechanical behaviors of 6061 al matrix hybrid composites reinforced with sic and stainless steel particles, Mater. Sci. Eng., A 804 (2021) 140732, https://doi.org/10.1016/j.msea.2021.140732.

[5] M.R. Rezaei, R. Nazemnezhad, S. Farahmandrad, Effects of the si element on the microstructure and mechanical properties of an al/fmg/sic hybrid composite, Mater. Chem. Phys. 309 (2023) 128343, https://doi.org/10.1016/j.matchemphys.2023.128343.

[6] S. Zhang, et al., Graphene/zro2/aluminum alloy composite with enhanced strength and ductility fabricated by laser powder bed fusion, J. Alloys Compd. 910 (2022) 164941, https://doi.org/10.1016/j.jallcom.2022.164941.

[7] S. Mahdavi, F. Akhlaghi, Effect of sic content on the processing, compaction behavior, and properties of al6061/sic/gr hybrid composites, J. Mater. Sci. 46 (2011) 1502, https://doi.org/10.1007/s10853-010-4954-x.

[8] M. Moazami-Goudarzi, F. Akhlaghi, Effect of sic nanoparticles addition on densification of commercially pure al and 5252 al powder compacts, J. Ultrafine Grained Nanostruct. Mater. 54 (2021) 121, https://doi.org/10.22059/jufgnsm.2021.02.01.

[9] M. Moazami-Goudarzi, F. Akhlaghi, Effect of nanosized sic particles addition to cp al and al–mg powders on their compaction behavior, Powder Technol. 245 (2013) 126, https://doi.org/10.1016/j.powtec.2013.04.025.

[10] F. Akhlaghi, A. Lajevardi, H.M. Maghanaki, Effects of casting temperature on the microstructure and wear resistance of compocast a356/sicp composites: a comparison between ss and sl routes, J. Mater. Process. Technol. 155–156 (2004) 1874, https://doi.org/10.1016/j.jmatprotec.2004.04.328.

[11] H. Ahmadian, et al., Investigating the valence balance of adding nano sic and mwcnts on the improvement properties of copper composite using mechanical alloying and sps techniques, Diam. Relat. Mater. 145 (2024) 111113, https://doi.org/10.1016/j.diamond.2024.111113.

[12] S. Mosleh-Shirazi, F. Akhlaghi, The impact of matrix microstructure and reinforcement size (micron vs. Nano-size) on the compressibility of al-sic powder mixtures and hardness of al/sic composites, J. Ultrafine Grained Nanostruct. Mater. 55 (2022) 133, https://doi.org/10.22059/jufgnsm.2022.02.05.

[13] H. Ahmadian, et al., Predicting crystallite size of mg-ti-sic nanocomposites using an adaptive neuro-fuzzy inference system model modified by termite life cycle optimizer, Alex. Eng. J. 84 (2023) 285, https://doi.org/10.1016/j.aej.2023.11.009.

[14] S.P. Dwivedi, V. Chaudhary, S. Sharma, Synergistic performance evaluation of copper–wc-graphene composites: microstructure, mechanical properties, corrosion, and wear behavior under microwave sintering, Mater. Chem. Phys. 317 (2024) 129202, https://doi.org/10.1016/j.matchemphys.2024.129202.

[15] S. Mosleh-Shirazi, F. Akhlaghi, D.-Y. Li, Effect of sic content on dry sliding wear, corrosion and corrosive wear of al/sic nanocomposites, Trans. Nonferrous Metals Soc. China 26 (2016) 1801, https://doi.org/10.1016/S1003-6326(16)64294-2.

[16] A. Malti, A. Kardani, A. Montazeri, An insight into the temperature-dependent sintering mechanisms of metal nanoparticles through md-based microstructural analysis, Powder Technol. 386 (2021) 30, https://doi.org/10.1016/j.powtec.2021.03.037.

[17] P. Eftekharimilani, F. Akhlaghi, Flake powder metallurgy approach for production of al–al2o3 composites with enhanced properties, Surf. Rev. Lett. 30 (2023) 2350007, https://doi.org/10.1142/S0218625X23500075.

[18] M.H. Adib, R. Abedinzadeh, Study of mechanical properties and wear behavior of hybrid al/(al2o3+sic) nanocomposites fabricated by powder technology, Mater. Chem. Phys. 305 (2023) 127922, https://doi.org/10.1016/j.matchemphys.2023.127922.

[19] K. Chu, C. Jia, Enhanced strength in bulk graphene–copper composites, Phys. Status Solidi (a) 211 (2014) 184, https://doi.org/10.1002/pssa.201330051.

[20] A. Fathy, A. Abu-Oqail, A. Wagih, Improved mechanical and wear properties of hybrid al-al2o3/gnps electro-less coated ni nanocomposite, Ceram. Int. 44 (2018) 22135, https://doi.org/10.1016/j.ceramint.2018.08.326.

[21] K. Hemalatha, et al., Experimental study on behaviour of sic and graphene on al7075 hybrid metal matrix composite, Mater. Today Proc. 39 (2021) 26, https://doi.org/10.1016/j.matpr.2020.05.744.

[22] F. Lin, et al., Synergistic effects of tic and graphene on the microstructure and tribological properties of al2024 matrix composites, Adv. Powder Technol. 32 (2021) 3635, https://doi.org/10.1016/j.apt.2021.08.015.

[23] S.K. Tripathy, A.K. Senapati, An extensive analysis of mechanical and tribological studies of al6061 alloy based hybrid composite reinforced with b4c and graphene, Mater. Today Proc. 44 (2021) 2808, https://doi.org/10.1016/j.matpr.2020.12.1148.

[24] K. Zheng, Sliding-wear behavior of aluminum-matrix composites reinforced with graphene and sic nanoparticles, Materiali in tehnologije 54 (2020) 41.

[25] Q.A. Shafqat, et al., Mechanical, tribological, and electrochemical behavior of hybrid aluminum matrix composite containing boron carbide (b4c) and graphene nanoplatelets, J. Mater. Res. 34 (2019) 3116, https://doi.org/10.1557/jmr.2019.242.

[26] M. Şenel, M. Gürbüz, Investigation on mechanical properties and microstructures of aluminum hybrid composites reinforced with al 2 o 3/gnps binary particles, Arch. Metall. Mater. 66 (2021), https://doi.org/10.24425/amm.2021.134764.

[27] S.F. Bartolucci, et al., Graphene–aluminum nanocomposites, Mater. Sci. Eng., A 528 (2011) 7933.

[28] X. Zeng, et al., Wear characteristics of hybrid aluminum-matrix composites reinforced with well-dispersed reduced graphene oxide nanosheets and silicon carbide particulates, Vacuum 155 (2018) 364, https://doi.org/10.1016/j.vacuum.2018.06.033.

[29] X. Du, et al., Fabrication and characterization of al 7075 hybrid composite reinforced with graphene and sic nanoparticles by powder metallurgy, Dig. J. Nanomater. Biostruct. 13 (2018) 1133, https://doi.org/10.1007/s00170-012-4200-6.

[30] M.S.G. Gol, A. Malti, F. Akhlaghi, Effect of wc nanoparticles content on the microstructure, hardness and tribological properties of al-wc nanocomposites produced by flake powder metallurgy, Mater. Chem. Phys. (2022) 127252, https://doi.org/10.1016/j.matchemphys.2022.127252.

[31] Y. Jiang, et al., Tailoring the structure and mechanical properties of graphene nanosheet/aluminum composites by flake powder metallurgy via shift-speed ball milling, Compos. Appl. Sci. Manuf. 111 (2018) 73, https://doi.org/10.1016/j.compositesa.2018.05.022.

[32] A. Hassan, et al., Effect of mechanical milling on the morphologyand structural evaluation of al-al2o3 nanocomposite powders, Int. J. Eng. 27 (2014) 625, https://doi.org/10.5829/idosi.ije.2014.27.04a.14.

[33] S. Khadem, S. Nategh, H. Yoozbashizadeh, Structural and morphological evaluation of al–5 vol.% sic nanocomposite powder produced by mechanical milling, J. Alloys Compd. 509 (2011) 2221, https://doi.org/10.1016/j.jallcom.2010.10.188.

[34] E. Ghandourah, et al., Comprehensive investigation of the impact of milling time on microstructural evolution and tribological properties in mg-ti-sic hybrid composites, Mater. Today Commun. 38 (2024) 107835, https://doi.org/10.1016/j.mtcomm.2023.107835.

[35] H. Ahmadian, et al., Utilizing a unified conceptual dynamic model for prediction of particle size of duel-matrix nanocomposites during mechanical alloying, Powder Technol. 418 (2023) 118291, https://doi.org/10.1016/j.powtec.2023.118291.

[36] N. Akçamlı, et al., Investigation of microstructural, mechanical and corrosion properties of graphene nanoplatelets reinforced al matrix composites, Mater. Res. Express 6 (2019) 115627, https://doi.org/10.1088/2053-1591/ab511f.
[37] T. Varol, A. Canakci, Microstructure, electrical conductivity and hardness of multilayer graphene/copper nanocomposites synthesized by flake powder metallurgy, Met. Mater. Int. 21 (2015) 704, https://doi.org/10.1007/s12540-015-5058-6.
[38] H. Asgharzadeh, H. Mcqueen, Grain growth and stabilisation of nanostructured aluminium at high temperatures, Mater. Sci. Technol. 31 (2015) 1016, https://doi.org/10.1179/1743284714Y.0000000706.
[39] R. Pérez-Bustamante, et al., Microstructural and hardness behavior of graphene-nanoplatelets/aluminum composites synthesized by mechanical alloying, J. Alloys Compd. 615 (2014) S578, https://doi.org/10.1016/j.jallcom.2014.01.225.
[40] A. Bisht, et al., Strengthening mechanism in graphene nanoplatelets reinforced aluminum composite fabricated through spark plasma sintering, Mater. Sci. Eng., A 695 (2017) 20.
[41] M. Khoshghadam-Pireyousefan, et al., Application of a novel method for fabrication of graphene reinforced aluminum matrix nanocomposites: synthesis, microstructure, and mechanical properties, Mater. Sci. Eng., A 772 (2020) 138820, https://doi.org/10.1016/j.msea.2019.138820.
[42] Pourmand N. Seyed, H. Asgharzadeh, Aluminum matrix composites reinforced with graphene: a review on production, microstructure, and properties, Crit. Rev. Solid State Mater. Sci. 45 (2020) 289, https://doi.org/10.1080/10408436.2019.1632792.
[43] F. Akhlaghi, S. Mahdavi, Effect of the sic content on the tribological properties of hybrid al/gr/sic composites processed by in situ powder metallurgy (ipm) method, Adv. Mater. Res. 264–265 (2011) 1878. https://doi.org/10.4028/www.scientific.net/AMR.264-265.1878.
[44] A. Sadoun, et al., Experimental study on properties of al–al2o3 nanocomposite hybridized by graphene nanosheets, J. Mater. Res. Technol. 9 (2020) 14708, https://doi.org/10.1016/j.jmrt.2020.10.011.
[45] V. Chenrayan, et al., Tribological performance of tib2-graphene al 7075 hybrid composite processed through squeeze casting: at room and high temperature, Tribol. Int. 185 (2023) 108486, https://doi.org/10.1016/j.triboint.2023.108486.
[46] R. Geng, F. Qiu, Q.C. Jiang, Reinforcement in al matrix composites: a review of strengthening behavior of nano-sized particles, Adv. Eng. Mater. 20 (2018) 1701089, https://doi.org/10.1002/adem.201701089.
[47] S.I. Ghazanlou, B. Eghbali, R. Petrov, Microstructural evolution and strengthening mechanisms in al7075/graphene nano-plates/carbon nano-tubes composite processed through accumulative roll bonding, Mater. Sci. Eng., A 807 (2021) 140877, https://doi.org/10.1016/j.msea.2021.140877.
[48] M.I. Elamy, et al., Enhanced random vector functional link based on artificial protozoa optimizer to predict wear characteristics of cu-zro2 nanocomposites, Result. Eng. 24 (2024) 103007, https://doi.org/10.1016/j.rineng.2024.103007.
[49] J. Li, X. Zhang, L. Geng, Effect of heat treatment on interfacial bonding and strengthening efficiency of graphene in gnp/al composites, Compos. Appl. Sci. Manuf. 121 (2019) 487, https://doi.org/10.1016/j.compositesa.2019.04.010.
[50] J. Wang, et al., Reinforcement with graphene nanosheets in aluminum matrix composites, Scr. Mater. 66 (2012) 594, https://doi.org/10.1016/j.scriptamat.2012.01.012.
[51] M.M. Tünçay, et al., Spark plasma sintering and spark plasma upsetting of an al-zn-mg-cu alloy, Mater. Sci. Eng., A 704 (2017) 154, https://doi.org/10.1016/j.msea.2017.08.015.
[52] A. Pal, et al., Tribological behavior of al-wc nano-composites fabricated by ultrasonic cavitation assisted stir-cast method, Mater. Res. Express 5 (2018) 036521, https://doi.org/10.1088/2053-1591/aab577.
[53] A. Bahri, et al., Mechanical and electrochemical behaviors assessments of aluminum-graphene oxide composites fabricated by mechanical milling and repetitive upsetting extrusion, J. Composit. Compound. 3 (2021) 152, https://doi.org/10.52547/jcc.3.3.1.
[54] E.D. Yalçin, A. Çanakçi, Corrosion and wear performance of za27/graphene/b4c hybrid nanocomposites produced by powder metallurgy, Acta Metallurgica Slovaca 26 (2020) 126, https://doi.org/10.36547/ams.26.3.538.
[55] J. Zhang, et al., Effect of graphene on the tribolayer of aluminum matrix composite during dry sliding wear, Surf. Coating. Technol. 358 (2019) 907, https://doi.org/10.1016/j.surfcoat.2018.11.065.
[56] A. El-Ghazaly, G. Anis, H.G. Salem, Effect of graphene addition on the mechanical and tribological behavior of nanostructured aa2124 self-lubricating metal matrix composite, Compos. Appl. Sci. Manuf. 95 (2017) 325, https://doi.org/10.1016/j.compositesa.2017.02.006.
[57] H. Khosravi, F. Akhlaghi, Comparison of microstructure and wear resistance of a356-sicp composites processed via compocasting and vibrating cooling slope, Trans. Nonferrous Metals Soc. China (2015), https://doi.org/10.1016/S1003-6326(15)63867-5.
[58] A.D. Moghadam, et al., Mechanical and tribological properties of self-lubricating metal matrix nanocomposites reinforced by carbon nanotubes (cnts) and graphene–a review, Compos. B Eng. 77 (2015) 402, https://doi.org/10.1016/j.compositesb.2015.03.014.
[59] W. Bollmann, J. Spreadborough, Action of graphite as a lubricant, Nature 186 (1960) 29, https://doi.org/10.1038/186029a0.
[60] D. Jun, et al., Dry sliding friction and wear properties of al2o3 and carbon short fibres reinforced al–12si alloy hybrid composites, Wear 257 (2004) 930, https://doi.org/10.1016/j.wear.2004.05.009.
[61] A. Nieto, et al., Oxidation behavior of graphene nanoplatelet reinforced tantalum carbide composites in high temperature plasma flow, Carbon 67 (2014) 398, https://doi.org/10.1016/j.carbon.2013.10.010.
[62] R. Mehta, S. Chugh, Z. Chen, Transfer-free multi-layer graphene as a diffusion barrier, Nanoscale 9 (2017) 1827, https://doi.org/10.1039/C6NR07637H.
[63] H. Ahmadian, et al., Microstructure, mechanical properties and wear behavior of mg matrix composites reinforced with ti and nano sic particles, J. Mater. Res. Technol. 31 (2024) 4088, https://doi.org/10.1016/j.jmrt.2024.07.125.
[64] I. Dinaharan, et al., Influence of particle content and temperature on dry sliding wear behavior of rice husk ash reinforced aa6061 slurry cast aluminum matrix composites, Tribol. Int. 183 (2023) 108406, https://doi.org/10.1016/j.triboint.2023.108406.
[65] W.-S. Kuo, N.-H. Tai, T.-W. Chang, Deformation and fracture in graphene nanosheets, Compos. Appl. Sci. Manuf. 51 (2013) 56, https://doi.org/10.1016/j.compositesa.2013.03.020.
[66] A. Mazahery, M.O. Shabani, Microstructural and abrasive wear properties of sic reinforced aluminum-based composite produced by compocasting, Trans. Nonferrous Metals Soc. China 23 (2013) 1905, https://doi.org/10.1016/S1003-6326(13)62676-X.
[67] H. Hocheng, et al., Fundamental turning characteristics of a tribology-favored graphite/aluminum alloy composite material, Compos. Appl. Sci. Manuf. 28 (1997) 883, https://doi.org/10.1016/S1359-835X(97)00055-9.
[68] M. Islam, et al., Microstructural evaluation of inductively sintered aluminum matrix nanocomposites reinforced with silicon carbide and/or graphene nanoplatelets for tribological applications, Metall. Mater. Trans. 49 (2018) 2963, https://doi.org/10.1007/s11661-018-4625-0.
[69] J. Archard, Contact and rubbing of flat surfaces, J. Appl. Phys. 24 (1953) 981, https://doi.org/10.1063/1.1721448.
[70] L.K. Pillari, K. Lessoway, L. Bichler, Reciprocating dry sliding friction and wear behavior of b319 aluminum alloy-graphene composites, Tribol. Int. 192 (2024) 109334, https://doi.org/10.1016/j.triboint.2024.109334.